Nanofiltration Membranes Prepared by Direct Microemulsion Copolymerization Using Poly(Ethylene Oxide) Macromonomer as a Polymerizable Surfactant

J. LIU,[1] W. K. TEO,[2] C. H. CHEW,[3] L. M. GAN[3]

[1] Technical Center, Union Carbide Asia Pacific, Inc., 16 Science Park Drive, No. 04-01/02 The Pasteur, Singapore 118227

[2] Department of Chemical Engineering, National University of Singapore, Singapore 119260

[3] Department of Chemistry, National University of Singapore, Singapore 119260

Received 16 November 1999; accepted 21 January 2000

ABSTRACT: A novel polymer membrane with nanosized pore structures has been prepared from the direct copolymerization of acrylonitrile (AN) with a polymerizable nonionic surfactant in water-in-oil (w/o) or bicontinuous microemulsions. This polymerizable surfactant is ω-methoxy poly(ethylene oxide)$_{40}$ undecyl-α-methacrylate macromonomer [CH_3O—$(CH_2CH_2O)_{40}$—$(CH_2)_{11}$—$OCO(CH_3)C$═CH_2, abbreviated: C_1-PEO-C_{11}-MA-40]. Besides PEO macromonomer, AN, and crosslinker ethyleneglycol dimethacrylate, the microemulsion system contained varying amount of water that formed w/o microemulsions having water droplet structures and bicontinuous microemulsions consisting of interconnected water channel. The polymerized membranes prepared in this study have pore radii ranging from 0.38 to 2.4 nm as evaluated by PEG filtration. The pore size appears to vary linearly with water content in precursor microemulsions. But a sharp change in the gradient of the linear relationship is observed around 25 wt % water content. Membranes made from bicontinuous (>25 wt % water) microemulsion polymerization have a larger and interconnected (open-cell) nanostructures. In contrast, much smaller closed-cell (disinterconnected) nanostructures were obtained from w/o (<25 wt % water) microemulsion polymerization and the membrane exhibited a permselectivity toward water in pervaporation separation of high ethanol (>50 wt %) aqueous solutions. The separation factor (α) for 95% ethanol aqueous solution by the membrane derived from the microemulsion containing 10 wt % water is about 20. © 2000 John Wiley & Sons, Inc. J Appl Polym Sci 77: 2785–2794, 2000

Key words: nanofiltration membranes; microemulsion copolymerization; polymerizable surfactant; nanostructure; pervaporation

INTRODUCTION

The flat-sheet membranes can be prepared from solvent cast processes.[1] Since this process needs to dry a polymer or copolymer solution to a polymeric film, the evaporation of organic solvents causes environmental pollution and makes it expensive. Huang et al.[2,3] have improved these by direct casting of polymer emulsions: a final latex membrane is applied to the pervaporation separation process for the dehydration of water–ethanol mixtures. Ruckenstein et al.[3–10] have developed a new method called "concentrated emulsion polymerization" for the preparation of hydropho-

Correspondence to: J. Liu.

Journal of Applied Polymer Science, Vol. 77, 2785–2794 (2000)

bic–hydrophilic composite membranes. The advantage of using a concentrated emulsion is that high dispersed phase volume fractions as large as 0.99 can be obtained for making efficient membranes for pervaporation use.

Most recently, the polymeric membranes have been prepared from microemulsion polymerization using nonpolymerizable surfactants[11,12] or polymerizable surfactants.[13] With the use of a polymerizable surfactant in the microemulsion system, all organic components are polymerizable. After polymerization, the polymerizable surfactant is chemically bonded in the resulting polymeric membrane. Thus, its membrane hydrophilicity is greatly enhanced by this solvent-free microemulsion polymerization in a single step.

In our previous papers,[14–18] we have reported a synthesized polymerizable surfactant, ω-methoxy poly(ethylene oxide)$_{40}$ undecyl-α-methacrylate macromonomer [CH_3O—$(CH_2CH_2O)_{40}$—$(CH_2)_{11}$—$OCO(CH_3)$ C═CH_2, or the abbreviation: C_1-PEO-C_{11}-MA-40]. It readily forms micelles that proceed unusually high rate of polymerization in aqueous media. The monodisperse polymer particles can readily be obtained via emulsion[17] or dispersion[15,16] polymerization using the C_1-PEO-C_{11}-MA-40 macromonomer as a polymerizable surfactant or polymerizable steric stabilizer. It can also be used to form transparent polymeric materials via a bicontinuous microemulsion polymerization[18] containing methyl methacrylate and 2-hydroxyethyl methacrylate (HEMA). It was found that the resulting polymer materials had interconnected (open-cell) nanostructures when the water content used in the microemulsion was varied from 25 to 60 wt %.

In this paper, the preparation and characterization of the nanofiltration membranes from the related microemulsion systems are reported and the pervaporation experiment on ethanol–water mixtures is also studied for the obtained membranes.

EXPERIMENTAL

Materials

Acrylonitrile (AN) and ethylene glycol dimethacrylate (EGDMA) were obtained from Aldrich and purified under reduced pressure. Ammonium persulfate (APS) from Fluka and *N, N, N′, N′*-tetramethylethylenediamine (TMEDA) from Aldrich were used as received. The Millipore water of

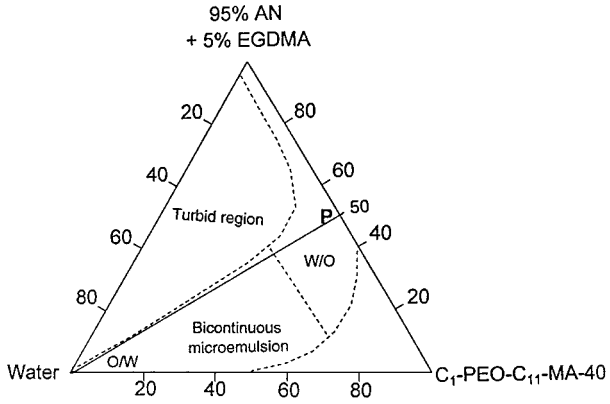

Figure 1 The phase diagram for the system of AN/EGDMA/C_1-PEO-C_{11}-MA-40/H_2O at 30°C. O/W: oil-in-water microemulsion; W/O: water-in-oil microemulsion and bicontinuous microemulsion.

electrical conductivity ca. 1.0 μs/cm was used. C_1-PEO-C_{11}-MA-40 macromonomer was prepared as reported early.[14] Polyethylene glycols (PEG) with different molecular weights were used as received from Aldrich.

Phase Diagram of Microemulsion

The clear regions of the microemulsion systems were determined visually by titrating a certain amount of AN, EGDMA, and C_1-PEO-C_{11}-MA-40 with water in a screw-capped tube at 30°C. EGDMA added was 5 wt % based on the total weight of AN. Each solution was thoroughly mixed using a Vortex mixer. The clear–turbid boundaries were established from the systematic titrations. The transparent microemulsion region is represented by the area enclosed by the dotted-line area as shown in Figure 1. The microemulsion region can further be classified as oil-in-water (o/w), bicontinuous and water-in-oil (w/o) microemulsions.

Polymerization and Membrane Preparation

The compositions (Table I) for membrane preparation from microemulsion polymerization were chosen from the microemulsion phase diagram (Fig. 1) along line P. The concentration of the redox initiator used was equimolar APS/TMEDA (10 m*M*/10 m*M*) on the basis of the water content.

Two 20 × 20 cm glass plates were washed and dried at room temperature. For the glass surfaces to be contacted with microemulsions, they were then polished using cotton with a small amount of silicon oil. This enables the easy removal of the

Table I Microemulsion Compositions[a] for Polymerization to Form Membranes

Microemulsion Samples	H_2O (wt %)	C_1-PEO-C_{11}-MA-40 (wt %)	Mixed Monomers[b] (wt %)	Gel Time at 30°C (min)
P-1	10	45.0	45.0	20
P-2	15	42.5	42.5	16
P-3	20	40.0	40.0	12
P-4	25	37.5	37.5	9
P-5	30	35.0	35.0	7
P-6	35	32.5	32.5	6

[a] Redox initiator consisted equimolar APS/TMEDA (10 m*M*/10 m*M*) based on the weight of water.
[b] The mixed monomers fixed at 95 wt % AN and 5 wt % EGDMA.

membrane after polymerization. About 4 g of each microemulsion was first prepared in a screw-capped tube and the polymerization started after TMEDA was added to the system with vigorous mixing using a mixer. The tube was ultrasonicated for 20 s to eliminate any tiny bubbles formed during mixing. The prepared microemulsion was then spread on the glass plate, and then slowly covered with another glass plate to avoid air bubble trapping. Small pieces of thin aluminum foil sheet were used as spacers in between the glass plates to regulate the membrane thickness. The polymerization in the glass plate assembly proceeded at 30°C for about 48 h. The casting assembly was opened in water and a translucent membrane was obtained. The thickness of the membranes was around 160 μm. The membranes were immersed in deionized water, which was changed daily for one week before testing.

Characterization of Membranes

Membrane Leaching

The membrane samples were dried under vacuum to constant weights. The dried samples were then extracted by hot water (oven at 50°C) for one week. Water was replaced once a day. The weight loss due to leaching was determined.

Glass Transition Temperature (T_g)

The T_g of each membrane was measured using a Dupont DSC2920 differential scanning calorimeter (DSC) with a heating rate of 10°C/min. The initial onset of the slope of the DSC curve was taken as T_g.

Equilibrium Swelling Ratio

After the membrane strips were completely dried in vacuum at room temperature until a constant weight was attained, the dried membrane was immersed in a water–ethanol mixture at 25°C until it reached the swelling equilibrium. The swollen membrane was then weighed after blotting off the liquid on its surface. The equilibrium swelling ratio (*ESR*) expressed as percentage is given by

$$ESR(\%) = \frac{W_s - W_d}{W_s} \times 100 \qquad (1)$$

where W_s and W_d denote the weight of the water swollen membrane and the dry membrane respectively. If the liquid is pure water, the *ESR* can also be expressed as *EWC* (equilibrium water content).

Drying Rate of Water Desorption

The drying rate of water desorption from membranes was monitored using a Dupont Instruments TGA 2960 thermogravimetric analyzer. The membrane was dried in a stream of dry nitrogen gas isothermally at 75°C for 5 h, before a temperature ramp of 2°C min^{-1} was applied until 100°C followed by keeping at this temperature for 1 h. The weight loss of the sample was recorded as a function of time throughout the experiment and the sample dimensions were measured again after drying. The drying rate for the polymer sample based on the average of the initial and final surface area was plotted against the free moisture content of the sample to yield the drying-rate curve.

Membrane Pore Size Evaluations

The pore size evaluation for the membranes was performed in test cells made of 316 stainless steel having the same configuration as those used by Sourirajan,[19] except that the effective membrane

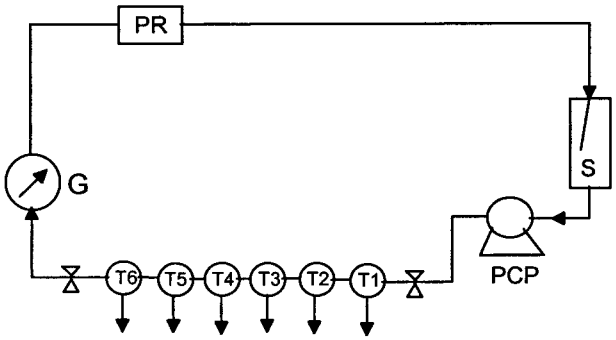

Scheme 1 The schematic diagram of an apparatus for membrane pore size evaluations. PCP, pressure control pump; T_i (i = 1–6), membrane test cells; G, pressure gauge; PR, pressure regulator; S, water or feed solution reservoir. The arrows marked in the figure show the direction of the fluid flow.

area used in this study was 14.85 cm^2. The membranes removed from the water bath were mounted onto stainless steel porous plates housed in the test cells. A porous filter paper was placed between the membrane and the porous plate to protect the membrane. The lower part of a test cell was a high pressure chamber provided with inlet and outlet opening for the flow of the feed solution. The upper part of a test cell had an outlet opening for the collection of the permeation product. The apparatus set-up for the pore size evaluation is shown in Scheme 1.

Before the test, Millipore water was circulated in the test loop for washing purposes. The feed solution containing the desired concentration of PEG was then passed through the test cells for solute rejection measurement.

The pore size of membranes can be estimated by the values of molecular weight cutoff (MWCO) using the Stokes–Einstein equation[20]:

$$r_a = (kT)/(6\pi\eta D_{AB}) \quad (2)$$

where r_a is the radius of different solutes of PEG, k Boltzmann's constant, T absolute temperature (K), η the viscosity (Pa · s) of water, and D_{AB} the diffusivity of the solute in water (cm^2/s), which can be found in ref. 21.

The membranes were operated at the average operating pressure of 400 psi at a flow velocity (100L/h). The PEG concentration in feed solution was maintained at 200 ppm in each testing experiment.

Solution concentrations in the feed and in the permeated product streams were determined using a Simadzu Total Carbon Analyzer Model-5000A. The percentage of PEG solute rejection, R_a was calculated from the following relation[20]:

$$R_a = [(C_b - C_p)/C_b] \times 100\% \quad (3)$$

where C_p and C_b are the permeate product concentration and the feed concentration of PEG respectively.

Pervaporation Experiments

The schematic setup for the pervaporation separation of water–ethanol mixtures is shown in Scheme 2. The cells were stainless steel chambers consisting of two detachable parts. Its upper part contained 250 mL of water–ethanol mixtures. The membrane was mounted on a stainless steel porous plate embedded in the lower part of the cell through which the membrane permeated vapor was withdrawn at a subatmospheric pressure (using a vacuum pump) at 5 ± 1 mbar. The two parts of the cell were screwed and sealed tightly using rubber O-ring. The effective membrane surface area was 14.85 cm^2.

The operation was performed at 25°C. The system was allowed to run for at least half an hour to reach steady state. The pervaporated vapor was then condensed in a cold trap of liquid nitrogen for a suitable period of time to ensure sufficient liquid being collected for analysis. The permeate compositions were analyzed by using Shimadzu Gas Chromatograph GC-14B with a thermal con-

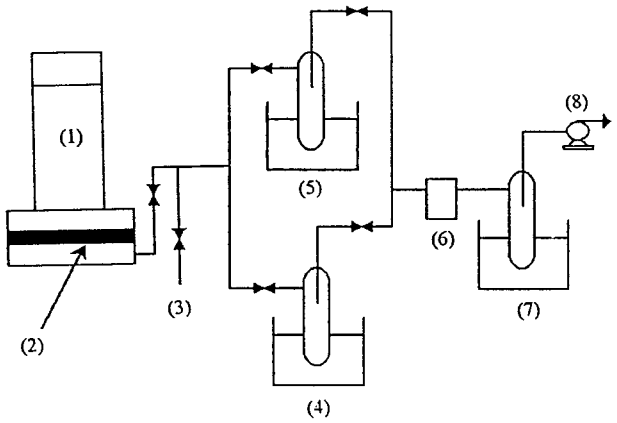

Scheme 2 Schematic diagram of the pervaporation separation apparatus. (1) pervaporation cell, (2) membrane, (3) pressure gauge, (4) and (5) cold traps, (6) vacuum controller, (7) protective cold trap, and (8) vacuum pump.

ductivity detector. The column temperature was 145°C using helium as the carrier gas.

Two factors were used for the evaluation of the membrane: (1) The permeation rate Q, expressed in g/m^2 h, was calculated from the amount of permeate collected for a specific duration of time through an effective membrane area. (2) The separation factor α was defined as

$$\alpha = \frac{Y_w/Y_e}{X_w/X_e} \quad (4)$$

where Y_w and Y_e represent the weight fractions of water and ethanol in the permeate and X_w and X_e those in the feed, respectively.

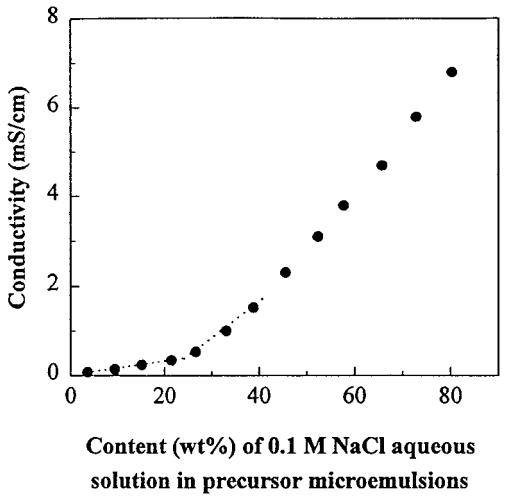

Figure 2 The change of conductivity of precursor microemulsions as a function of 0.1*M* NaCl aqueous solution along the composition line P of Figure 1.

RESULTS AND DISCUSSION

Microemulsion Systems

Besides the macromonomer C_1-PEO-C_{11}-MA-40 as a polymerizable nonionic surfactant, the systems also consisted of monomer AN, crosslinker EGDMA and water. These component formed a rather large transparent microemulsion region (area enclosed by dotted lines) as shown in Figure 1. Along the composition line P, the weight ratio of the monomers to C_1-PEO-C_{11}-MA-40 was fixed at 50:50. The monomers contained 95% AN and 5% EGDMA. By increasing the water content along the composition line P, some microemulsions were chosen, as listed in Table I, for the preparation of membranes.

There are three main types of microemulsions, namely o/w microemulsion, w/o, and bicontinuous microemulsion. The former two types of microemulsions possess o/w and w/o droplets, respectively, while the latter consists of bicontinuous microstructures where organic and aqueous phases coexisted in interconnected domains with surfactant molecules mostly confined to the oil–water interface. It is generally observed that w/o microemulsion form at lower aqueous content (<20 wt %). On the other hand, o/w microemulsions can be obtained at higher aqueous content (80 wt %). At the intermediate aqueous contents, bicontinuous structures may prevail. A conductivity measurement has been commonly used in identifying the type of microstructures for an ionic microemulsion. It is known that w/o and o/w microemulsions show very low and very high conductivity respectively. The transition from a w/o to a bicontinuous microemulsion would exhibit a rapid increase in conductivity.

Since the components of AN/EGDMA/C_1-PEO-C_{11}-MA-40/H_2O microemulsions are not conductive, 0.1*M* NaCl aqueous solution instead of water was used in the microemulsions for the purpose to roughly indicate the regions of w/o and bicontinuous microemulsions by conductivity measurements along the composition line P in Figure 1. Figure 2 shows the low conductivity of microemulsions at lower aqueous solutions (<25%), followed by a rapid increase in conductivity when the aqueous solution was greater than 25%. The low conductivity for the systems containing less than 25 wt % aqueous solution is attributed to the formation of w/o microemulsion droplets dispersed in the oil medium. The sharp increase in conductivity for the systems containing more than 25 wt % aqueous solutions denotes the presence of numerous interconnected conducting channels, which are the characteristics of bicontinuous microemulsions. Hence, we do not attempt to establish the boundary between bicontinuous microemulsion and o/w microemulsion. This is because our investigation focused on microemulsions containing less than 40% water as those compositions listed in Table I. It is inferred that samples P-1, P-2, and P-3 are w/o microemulsions while samples P-4, P-5, and P-6 are bicontinuous microemulsions. Membranes made from bicontinuous microemulsions with water contents larger than 40 wt % were mechanically weak.

Table II Equilibrium Water Content (*EWC*) of Each Membrane and Their Glass Transitions of Temperatures (T_g) and Weight Losses after Leaching

Sample No.	P-1	P-2	P-3	P-4	P-5	P-6
EWC (%)	22.1	27.0	32.8	39.5	45.7	52.3
Weight loss (wt %)	1.3	1.7	2.4	2.5	2.8	3.1
T_g (°C)						
T_{g1}	−50.9	−49.3	−50.2	−51.3	−50.3	−50.6
T_{g2}	74.6	73.8	74.1	73.5	74.8	74.1

Membrane Preparation

The polymerization of these microemulsions was initiated by a very active redox initiator composed of an equimolar of APS and TMEDA at 30°C. The fast gelation of these microemulsions could be achieved with 20 min (Table I). Since the aqueous phase contained 10 m*M* each of APS and TMEDA, the increasing gelation rate with the aqueous content in each microemulsion was due to the increasing amount of initiator used. The fast gelation of the microemulsions containing the polymerizable surfactant C_1-PEO-C_{11}-MA-40 is important for producing transparent polymeric materials without phase separation. This is because the possible rearrangements of the microstructures of microemulsions are thus minimized by the fast gelation during the early stage of polymerization. All the fluid microemulsion samples eventually transformed into translucent membranes. If the water content is less than 10 wt % in the precursor microemulsion, the system can not fully polymerize into membrane. This may be due to the insufficient amount of initiator existed in the system. If adding more initiator, the system becomes turbid and the phase separation will occur.

Table II shows that only about 1–3 wt % of polymerized membranes could be leached out after one week of hot water treatment at 50°C. This indicates that these microemulsions were almost completely copolymerized to form polymer networks in the form of membranes. Two glass transition temperatures (T_g) have been observed for these membranes. Its high T_{g2} (about 74°C) is due to the hydrophobic backbone of the copolymer (T_g for polyacrylonitrile is 104°C), whereas the low T_{g1} (about −50°C) is attributed to its long pendant groups of hydrophilic PEO. These membranes were mechanically strong enough for carrying on PEG filtration and pervaporation experiments.

The *EWC* for these membranes (Table II) increased with increasing amount of water in precursor microemulsions. This is because the porosity of these membranes increased with the increase of the water content in precursor microemulsions as has been observed for the polymerized C_1-PEO-C_{11}-MA-40 microemulsion system.[22] The results of all *EWC* were larger than the corresponding water contents in their precursor microemulsions. This means that the polymer substrates also adsorbed some water due to their hydrophilicity, in addition to those water already presented in the water pores or channels.

Characterization of Membranes

The water desorption from the membranes was studied by thermogravimetric analysis (TGA). The results from TGA are presented in Figure 3. Curves P-1 and P-3 illustrates the drying rate for the corresponding membranes made from w/o microemulsion samples P-1 and P-3 that contained

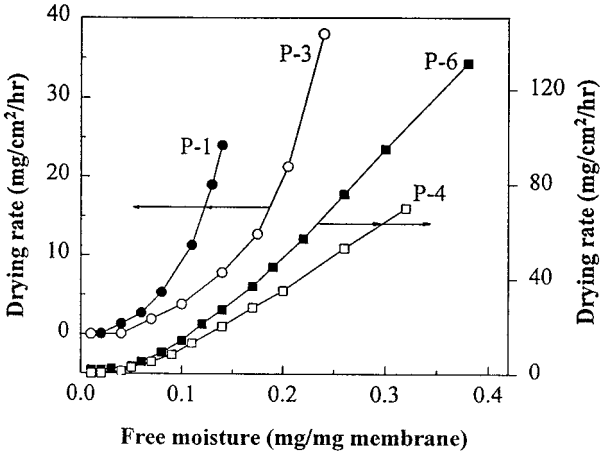

Figure 3 The drying rate curves for membranes made from microemulsion samples P-1, P-3, P-4, and P-6.

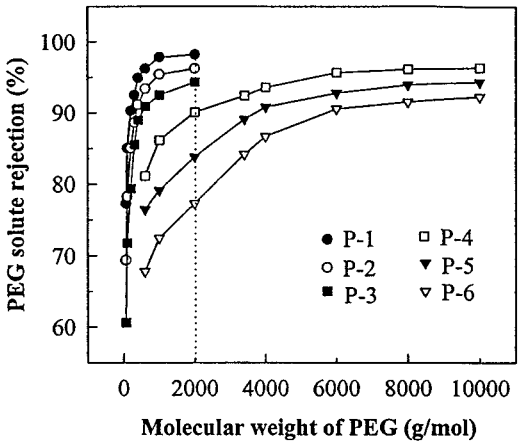

Figure 4 The PEG solute rejection by the synthesized membranes as a function of different PEG molecular weights.

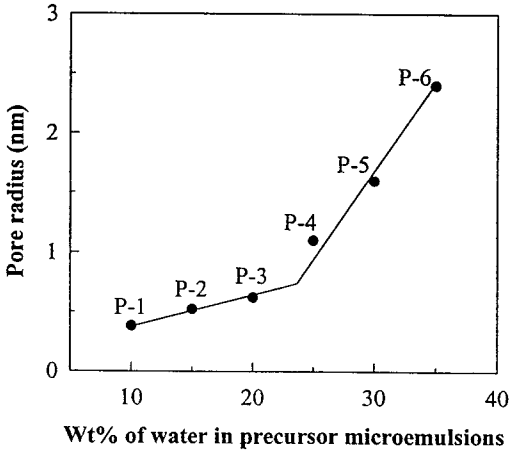

Figure 5 The dependence of pore sizes of the synthesized membranes on the water content of precursor microemulsions.

10 and 20 wt % water, respectively. The exponential falling rate period exhibited by membranes P-1 and P-3 is typical for the closed-cell porous structure which may be derived from the water domains (droplets) of their precursor w/o microemulsions. On the other hand, membranes P-4 and P-6 show an initial linear falling rate period in the higher free moisture region followed by an exponential decay, a behavior typical for open-cell porous materials.[23,24] Thus, the membranes obtained from samples P-1 to P-3 are believed to have disinterconnected porous structures, while membranes made from samples P-4 to P-6 could have an interconnected porous (channel or sponge-like) structure.

The pore sizes of the membranes were evaluated by PEG filtration experiments illustrated in Scheme 1. Figure 4 shows the PEG solute rejection as a function of PEG molecular weight for membranes P-1 to P-6. The percentage of PEG rejection (R_a) in each membrane increased with the increase of PEG molecular weights. At a given PEG molecular weight, R_a increased with decreasing water content in precursor microemulsions. For example, R_a at PEG 2000 decreased from 98% for sample P-1 to 77% for sample P-6 as the water content in the precursor microemulsion was increased from 10 to 35 wt %. This indicates that the membranes made from precursor microemulsions with different water contents have different pore sizes. The values of molecular weight cutoff (MWCO) for all membranes were obtained from those with 90% PEG rejection. Table III records the values of PEG MWCO and the pore radius of each membrane calculated from eq. (2). It was found that the pore radius of these membranes increased from 0.38 to 2.4 nm as the water content was increased from 10 to 35 wt %. The pore sizes of these membranes may be related to the sizes of water domains (droplets) and water channels in precursor w/o and bicontinuous microemulsions respectively.

The dependency of pore sizes of membranes on the water content in precursor microemulsions is also illustrated in Figure 5. The pore radius appears to increase linearly with the water content in precursor microemulsions in two region. In the region of below 25 wt % water content, the pore size of membrane was smaller and it gradually

Table III MWCOs of PEG from the Filtration[a] by Different Membranes and Their Respective Calculated Pore Size

Sample No.	P-1	P-2	P-3	P-4	P-5	P-6
MWCO (g/mole)	200	400	600	2000	4000	6000
Pore size (nm in radius)	0.38	0.52	0.62	1.1	1.6	2.4

[a] Operating pressure at 400 psi.

increased from 0.38 to 0.62 nm as the water content increased from 10 to 20 wt %. One may infer that the disinterconnected nanosized pores in membranes P-1, P-2, and P-3 may derive from the water domains (droplet) present in precursor w/o microemulsions. On the other hand, the pore size increased sharply from 1.1 to 2.4 nm with the increase of water content in precursor microemulsions from 25 to 35 wt %, as also reflected by the sharp increase in conductivity. Thus, the pore structures in polymerized membranes P-4, P-5, and P-6 are envisaged to be interconnected as the water channels (one of the bicontinuous phases) in precursor bicontinuous microemulsions.

The interconnected pore structures in membranes P-4, P-5, and P-6 (1.1–2.4 nm in radius) are much smaller than those (25–35 nm in radius) prepared from bicontinuous microemulsion polymerization using polymerizable zwitterionic surfactant (CH_2═$CHCOO(CH_2)_{11}N^+(CH_3)_2CH_2CH_2COO$-, AUDMAA).[25] Since C_1-PEO-C_{11}-MA-40 has a large hydrophilic group of 40 EO units, the water channels could be partially occupied by these polar groups of the macromonomers that are situated along the water/monomer interfaces. These PEO may still remain in the water channels after polymerization resulting in reducing the widths of water channels, in contrast to the zwitterionic AUDMAA system. Moreover, owing to the high solubility of monomer AN in water (7.8 wt %), AN may not only be polymerized in oil phase but also present in water channels of bicontinuous microemulsions. Once the microemulsion is polymerized, the deposition of water-swollen PAN or its copolymers in the water channels could narrow the bicontinuous nanostructure of the water channels. It has been found recently that HEMA can drastically reduce the pore size of coated membranes from AUDMAA bicontinuous microemulsion system due to its high solubility in water.[26]

Pervaporation Experiments

The pervaporation process is potentially useful when a distillation is difficult to apply, such as the separation of azeotropic mixtures, close-boiling point components, isomers, and for the removal or recovery of trace substances.[27–30] In a pervaporation experiment, the feed mixture is in direct contact with one size of a selective membrane, while the permeate is removed in the vapor state from the opposite side, which is kept under vacuum.[31] The liquid transport in pervaporation through the membrane takes place in three consecutive steps. The permeant is first sorbed at the interface between the feed solution and membrane, then it diffuses to the downstream side due to the concentration gradient of the individual permeant and desorbs into the vapor phase at the permeate side of the membrane. Among the three steps, desorption of the permeant is rapid, because, as long as the pressure in the permeate side is kept low, the rate of evaporation is high. Thus, the permeation rate (flux) and separation factor (selectivity) are mainly determined by the sorption and diffusion that are closely related to the membrane characteristics.

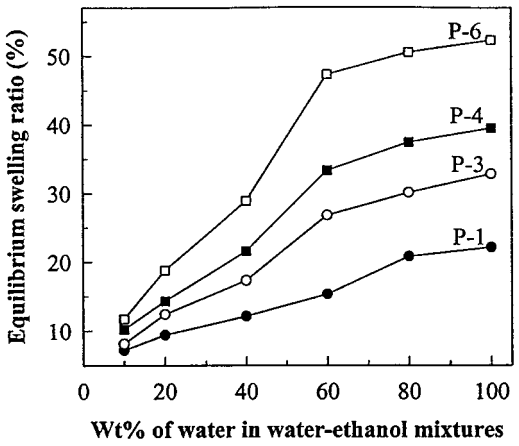

Figure 6 The equilibrium swelling ratios of some membranes in water–ethanol mixtures.

The *ESR*s of membranes P-1, P-3, P-4, and P-6 in different water–ethanol mixtures are shown in Figure 6. The *ESR* of each membrane increased with increasing amount of water in the water–ethanol mixture. Owing to the introduction of hydrophilic PEO groups of the macromonomer in microemulsions containing AN, the hydrophilicity of the polymerized membranes was greatly enhanced. The stronger membrane sorption at a higher water concentration of alcohol solution may be due to the higher affinity of the hydrophilic membranes for water than for ethanol. At a given alcohol concentration, the *ESR* of the membrane increases from the samples P-1 to P-6 as that for *EWC* in pure water. This is attributed to the increased porosity of membranes with increasing water content in precursor microemulsions.[22]

Figure 7 presents the dependence of separation factors (α) of membranes on the water content of precursor microemulsions for the pervaporation separation of 95 wt % ethanol aqueous solution at room temperature. Membranes P-4, P-5, and P-6

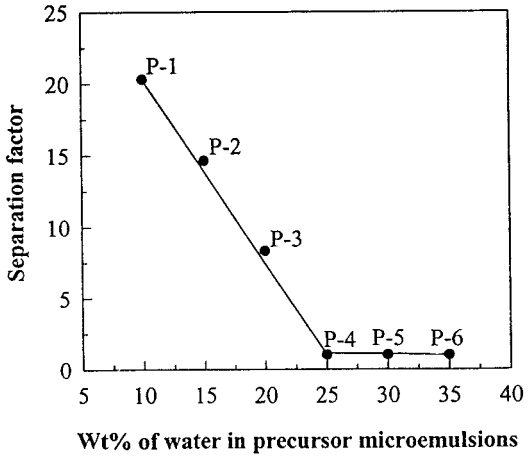

Figure 7 The dependence of separation factors of membranes on the water content of precursor microemulsions in pervaporation of 95 wt % ethanol aqueous solution.

have a negligible pervaporation separation factor ($\alpha \cong 1$). Since membranes possessed interconnected pore nanostructures larger than the molecular sizes of both ethanol and water, no separation can be obtained. On the other hand, membranes P-1, P-2, and P-3 made from the w/o microemulsion polymerization show the separation of water from the water–ethanol mixtures where α increased markedly from membranes P-4 to P-1. This is because membranes P-1, P-2, and P-3 have disinterconnected (closed-cell) pore structures and they exhibited permselective characteristics toward water by the selective sorption and diffusion.

The effect of ethanol concentrations in the feed on permeation rate and separation factor at room temperature is shown in Figures 8(a) and (b). The permeation rate decreased while the separation factor increased with increasing ethanol concentration in the feed. A pronounced increase in α was observed when the ethanol concentration was larger than 80 wt %. A negligible separation for ethanol concentration less than 50 wt % indicates water is selectively permeated only in the higher ethanol concentration range. This is because the PEO groups of these microemulsion membranes have strong interactions with water, which caused an extensive swelling of membranes in higher water (lower ethanol) concentration. The swollen pores of membranes would not only increase the permeation rate for water but also for ethanol, resulting in low separation. Thus the permeation rate was increased at the expense of the separation efficiency with the increase of water concentration in feeds.

At a given feed composition, membrane P-3 of larger pore size showed the largest permeation rate while membrane P-1 exhibited the biggest separation factor. As a result, the permeation rate for these membrane decreases in the order P-3 > P-2 > P-1, but the separation factor is in a reverse order, i.e., P-1 > P-2 > P-3. It is concluded that membrane P-1 is the best among the membranes prepared from microemulsion polymerization for this pervaporation study. Its highest value of αQ, was 11.2 kg/m^2 h, i.e., α and Q are 20.3 and 552 g/m^2 h, respectively.

CONCLUSION

Nanofiltration membranes were directly prepared from microemulsion copolymerization of acrylonitrile and a PEO polymerizable surfactant. The nanosized pore structure of membranes may be related to water-droplet domains or intercon-

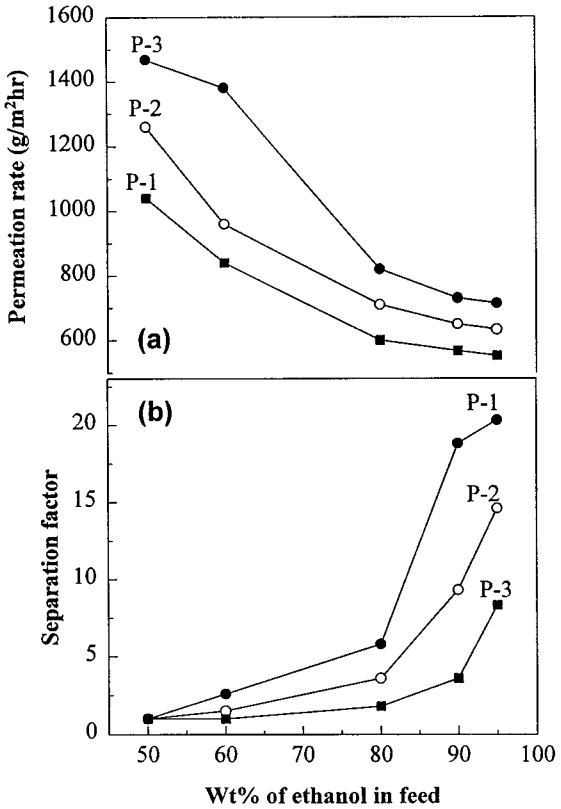

Figure 8 The effect of ethanol feed concentrations on the permeation rate and separation factor at room temperature.

nected water channels in their respective precursor w/o and bicontinuous microemulsions. The membrane hydrophilicity was greatly enhanced by the presence of hydrophilic PEO groups. The pore radius of the polymerized membranes ranged from 0.38 to 2.4 nm as the water content in precursor microemulsions was increased from 10 to 35 wt %, respectively. Below 25 wt % water content in the microemulsions, the pores obtained were disinterconnected and they became slightly larger at higher water contents. Above 25 wt % water content, the pores formed from bicontinuous microemulsions were interconnected and the pore size rapidly increased with water content. Membranes prepared from w/o microemulsion copolymerization were water selective in the pervaporation of high ethanol-content aqueous solutions. Their permeation rate was increased while the separation factor was decreased with increasing water concentration over concentrated ethanol feed solutions. The membrane prepared from its precursor w/o microemulsion at 10 wt % water exhibited better performance of pervaporation separation for 95% ethanol aqueous solution with the highest value of αQ being 11.2 kg/m^2 h.

REFERENCES

1. Porter, M. C. Handbook of Industrial Membrane Technology; Noyes Publications: Park Ridge, NJ; 1990.
2. Wei, Y.; Huang, R. Y. M. J Membrane Sci 1993, 82, 27.
3. Huang, R. Y. M.; Mei, Y. J Membrane Sci 1994, 87, 257.
4. Ruckenstein, E. Coll Polym Sci 1989, 267, 792.
5. Ruckenstein, E. Chen, H. H. J Membrane Sci 1992, 66, 205.
6. Ruckenstein, E.; Sun, F. J Appl Polym. Sci 1992, 46, 1271.
7. Ruckenstein, E.; Sun, F. J Membrane Sci 1993, 81, 191.
8. Ruckenstein, E.; Li, H. Polymer 1994, 35, 4343.
9. Sun, F.; Ruckenstein, E. J Membrane Sci 1995, 99, 273.
10. Ruckenstein, E.; Sun, F. J Membrane Sci 1995, 103, 271.
11. Palani Raj, W. R.; Sasthav, M.; Cheung, H. M. Polymer 1993, 34, 3305.
12. Cheeng, T. H.; Gan, L. M.; Teo, W. K.; Pey, K. L. Polymer 1996, 37, 5917.
13. Li, T. D.; Gan, L. M.; Chew, C. H.; Teo, W. K.; Gan, L. H. Langmuir 1996, 12, 5863.
14. Liu, J.; Chew, C. H.; Gan, L. M. J Macromol Sci-Chem 1996, A33(3), 337.
15. Liu, J.; Chew, C. H.; Wong, S. Y.; Gan, L. M.; Lin, J.; Tan, K. L. Polymer 1998, 39, 283.
16. Liu, J.; Gan, L. M.; Chew, C. H.; Gong, H.; Gan, L. H. J Polym Sci Part A Polym Chem 1997, 35, 3575.
17. Liu, J.; Chew, C. H.; Gan, L. H.; Teo, W. K.; Gan, L. M. Langmuir 1997, 13, 4988.
18. Gan, L. M.; Liu, J.; Poon, L. P.; Chew, C. H.; Gan, L. H. Polymer 1997, 38, 5339.
19. Sourirajan, S.; Matsuura, T. Reverse Osmosis/Ultrafiltration Process Principle; National Research Council of Canada, Toronto, 1985; p 79.
20. Kim, K. J.; Fane, A. G.; Aim, R. B.; Liu, M. G.; Jonsson, G.; Tessaro, I. C.; Broek, A. P.; Bargeman, D. J Membrane Sci 1994, 87, 35.
21. Sourirajan, S.; Matsuura, T. Reverse Osmosis/Ultrafiltration Process Principle; National Research Council of Canada, Toronto, 1985; p 688.
22. Liu, J.; Gan, L. M.; Chew, C. H.; Teo, W. K.; Gan, L. H. Langmuir 1997, 13, 6421.
23. McCabe, W. L.; Smith, J. C.; Harriot, P. Unit Operation of Chemical Engineering, 4th ed.; McGraw-Hill: New York, 1985; p 260.
24. Palani Raj, W. R.; Sasthav, M.; Cheung, H. M. J Appl Polym Sci 1993, 47, 499.
25. Gan, L. M.; Li, T. D.; Chew, C. H.; Teo, W. K.; Gan, L. H. Langmuir 1995, 11, 3316.
26. Li, T. D.; Gan, L. M.; Chew, C. H.; Teo, W. K.; Gan, L. H. J Membrane Sci 1997, 133, 177.
27. Seok, D. R.; Kang, S. G.; Hwang, S.-T. J Membrane Sci 1987, 33, 71.
28. Bddeker, K. W.; Bengston, G.; Pingel, H. J Membrane Sci 1991, 54, 1.
29. Mulder, M. H. V.; Kruitz, F.; Smolders, C. A. J Membrane Sci 1992, 11, 349.
30. Blume, I.; Wijmans, J. G.; Baker, R. W. J Membranes Sci 1990, 49, 253.
31. Kedem, O. In Proceedings of the First International Conference on Pervaporation Process in the Chemical Industry; Bakish, R., Ed.; Bakish Material Corp: New York, 1986; p 111.